Duan *et al.*
Chinese Journal of Mechanical Engineering (2022) 35:107
https://doi.org/10.1186/s10033-022-00772-7

Chinese Journal of Mechanical Engineering

ORIGINAL ARTICLE

Open Access

Precision and Flexible Bending Control Strategy Based on Analytical Models and Data Models

Yongchuan Duan[1,2], Le Tian[1,2], Fangfang Zhang[1,2*], Yu Liu[1,2], Haidi Qiao[1,2], Liu Yang[1,2] and Yingping Guan[1,2]

Abstract

Forming of various customized bending parts, small batches, as well as numerous types of materials is a new challenges for Industry 4.0, the current control strategies can not meet the precision and flexibility requirement, expected control strategy of bending processes need to not only resist unknown interferences of process condition and models, but also produce various new parts automatically and efficiently. In this paper, a precision and flexible bending control strategy based on analytical models and data models is proposed to build adaptive bending systems. New analytical prediction models for loading and unloading are established and suitable for various materials, a sequential identification strategy is proposed to search nominal properties using the four sub-optimization models. A data-based feedback model is established to prevent over-bending and eliminate online deviation. Above models are merged into a precision and flexible control strategy. The system firstly uses sub-optimization models to search the nominal point which is near to target point, secondly the system further uses feedback model to eliminate residual error between the nominal point and target point. Compared with four kinds sheet metals, the allowable ranges for variables are determined for a good convergence. The target bending angles were set to 20°, 40°, and 60°. Forty parts were tracked for each kind material, the adaptive bending system converged after one iteration, and exhibited better performances.

Keywords: Air bending, Springback control, Flexible bending control, Feedback compensation

1 Introduction

Owing to flexibility of the air bending process [1], it is widely used in the bending of sheets, pipes, and profiles [2–4]. This approach can be used to form multi-shaped parts by controlling the punch stroke [5], and many scholars have proposed automatic control methods [6]. With development of Industry 4.0 and artificial intelligence, process is more closely integrated to production lines [7]. If parts change, the equipment can adjust the process parameters adaptively. To deal with the diversification of materials and part shapes, as well as the interference from production lines [8–10], novel flexible predication models are urgently needed.

At present, many scholars propose analytical models, which are based on constraint mechanical equations that can easily reflect the internal mechanism. Stelson et al. [11] proposed a method to determine the related parameters of the sheet using the force–stroke curve, and then used identified material properties to calculate the subsequently process parameters. Moreover, Stelson [12] developed a recognition system with a better real-time performance. Stelson [13] further studied the adaptive control for strain-hardened materials. Antonelli et al. [14] use a simplified model to conduct identification. Ton et al. [15] studied strip metal bending based on his model. Dallinger et al. [16] established an air bending

*Correspondence: fangfang.zhang@ysu.edu.cn

[1] Key Laboratory of Advanced Forming & Stamping Technology and Science, Ministry of Education of China, Yanshan University, Qinhuangdao 066004, China
Full list of author information is available at the end of the article

control strategy through a two-step method based on a simplified model. Wang et al. [17] controlled the springback based on a simplified model. Presently, most scholars use simplified model to describe the loading process, which is difficult to precisely describe the behavior of various materials. If the bending deformation is not fully described by the hypothesis model, the control algorithm can not precisely and flexibly find the best working point. In addition, the research on unloading model is rare.

Actually, it is very difficult to thoroughly build bending model based on mechanical principles [18], and some assumptions have to be introduced. These assumptions and other unmodeled residuals cause deviations of prediction results [5]. Thus, many scholars have built models based on online data to predict bending process parameters [19]. Online data can include online interference, some is non-measurable, such as changes in lubrication conditions, tool wear, and equipment temperature rise, these can cause poor product consistency [20]. Many scholars use the feedback method to eliminate the deviation. Peter et al. [21] established a simplified control model for the blanking and bending processes based on the product chain, and realized the feedforward and feedback control of bending springback. Zafer [22] directly used experimental methods to generate data, and then performed springback control. Hazra et al. [23] studied the effects of changes in materials and processes on product formability. Some interference is measurable, such as material property fluctuation, if which can be evaluated in advance, the measurement data can be used to control the bending process. Therefore, many scholars used feedforward control methods to control the process. Havinga et al. [24] used bending force for feedforward control, and realized the consistency control of the product by product fluctuation. Yang et al. [25] used an online database and a fuzzy control model to regulate the precision bending process. Longo et al. [26] used control algorithms to predict bending springback in advance. Lewin et al. [27] used the feedforward control method to identify and control system. Yang et al. [28] developed an intelligent bending process based on a feedforward control system. Groche et al. [29] identified property based on statistical models, and then, controlled the bending process. From above analysis, it is relatively easy to fit a springback feedback model using online data, such as above feedforward and feedback models, But which need to accumulate a certain amount of data. In addition, when a model go beyond data boundary, the extrapolation accuracy of this model is poor [30, 31]. If the target angle of control system is repeatedly adjusted within a wide range, a large amount of data collected from history record are required to fit the model, as a result, a lot of discarded parts are produced. So the disadvantages of the fitting model from online data are obvious, a feedback model based on data from the analytical model will be researched. In this paper, the first originality lies that new analytical prediction models for loading and unloading are established for applicability with various materials, and the sequential identification strategy is proposed to search nominal properties of sheet metal automatically, based on this fact, flexible control is realized. The second originality lies that a data-based feedback model is established to prevent over-bending and eliminate online deviation from optimized point, in this way, precision control is realized.

Research on precision and flexible bending control strategy is the focus herein. The advances of this article are as follows: Firstly, in response to the material diversity problem, novel prediction models are established to ensure the applicability, and a sequential identification strategy is proposed to search nominal properties of sheet metal to be manufactured for each of the four sub-optimization problems, so flexible control can be done automatically. Secondly, a data-based feedback model is established to eliminate online deviation from optimized point, whose parameter within a certain safety margin is given to ensure that part is not over-bending, so precision control can be achieved steadily. Thirdly, the control strategy of the flexible system is finally determined as two steps. Step one is that the system uses sub-optimization models to search the nominal point which is near to target point, then step two is that the system further uses feedback model to eliminate residual error between the nominal point and target point. Last but not least, the flexible system convergence effect using this control strategy is verified by experiments.

2 Analytical Models and the Parameters Identification Strategy

2.1 Flexible Hardening Model for Sheet Metal

To improve the adaptability of the flexible system, the material hardening model which have a wider description capability will be selected preferentially. From references, one type is constructed in the form of a power function, while the other is in the form of an exponential function. Among the power function type are the Hollomon and Ludwik models, whereas the exponential function models include the Voce, Voce+Voce, Voce++, and Hockett–Sherby models. The Ludwik type is an improved variant of the Hollomon model. The power function model is usually an unsaturated one, while the Voce type is saturated, and the other exponential function models are variants of the Voce model. So Ludwik model and Voce model are recommended firstly. So the first recommended elementary function is determined by referring to the Ludwik constitutive equation as presented thus:

$$\sigma = \begin{cases} E\varepsilon, & \varepsilon \le \varepsilon_s, \\ \sigma_s + K\left(\varepsilon^n - \varepsilon_s^n\right), & \varepsilon \ge \varepsilon_s, \end{cases} \tag{1}$$

where σ is true stress, ε is true strain, E is elastic modulus, ε_s is yield strain, σ_s is yield strength, K is strength coefficient, and n is hardening index. Referring to the Voce constitutive equation, the second recommended elementary function is determined as follows:

$$\sigma = \begin{cases} E\varepsilon, & \varepsilon \le \varepsilon_s, \\ \sigma_s + A[\exp(-B\varepsilon_s) - \exp(-B\varepsilon)], & \varepsilon \ge \varepsilon_s, \end{cases} \tag{2}$$

where A and B are Voce model coefficients.

In order to test the hardening models, three representative curves are selected, as shown in Figure 1. High-strength steel DP980 have a higher yield stress, lower uniform elongation, and no evident yield turning point. The aluminum alloy 6061 sheets exhibits an apparent elastic-plastic transition. With the continuation of plastic deformation, the material hardening rate decreases slowly in a small range. For the 304 stainless steel material, there is a visible elastic–plastic transition curve, the hardening rate of the material, which remains larger than those of the other two, changes a little. Other test materials with similar behaviors are not listed there individually.

After fitting the stress and strain data of the material by the above two elementary functions, the fitting results are shown in the Figure 1(b)–(d). DP980 sheet metal is better fitted by Voce model than Ludwik model. The correlations of Voce model and Ludwik model with aluminum alloy 6061 sheet are similar. For the 304 stainless steel, it is same as aluminum alloy 6061 sheet.

When the elementary functions are used to extrapolate the high strain data, the Voce hardening rate changes little and tends to be saturated earlier, while the Ludwik model can continue to harden and be consistent with the cold working hardening behavior of the material. Therefore, when the material hardens slowly, the Ludwik and Voce models can be linearly combined to build a flexible hardening model:

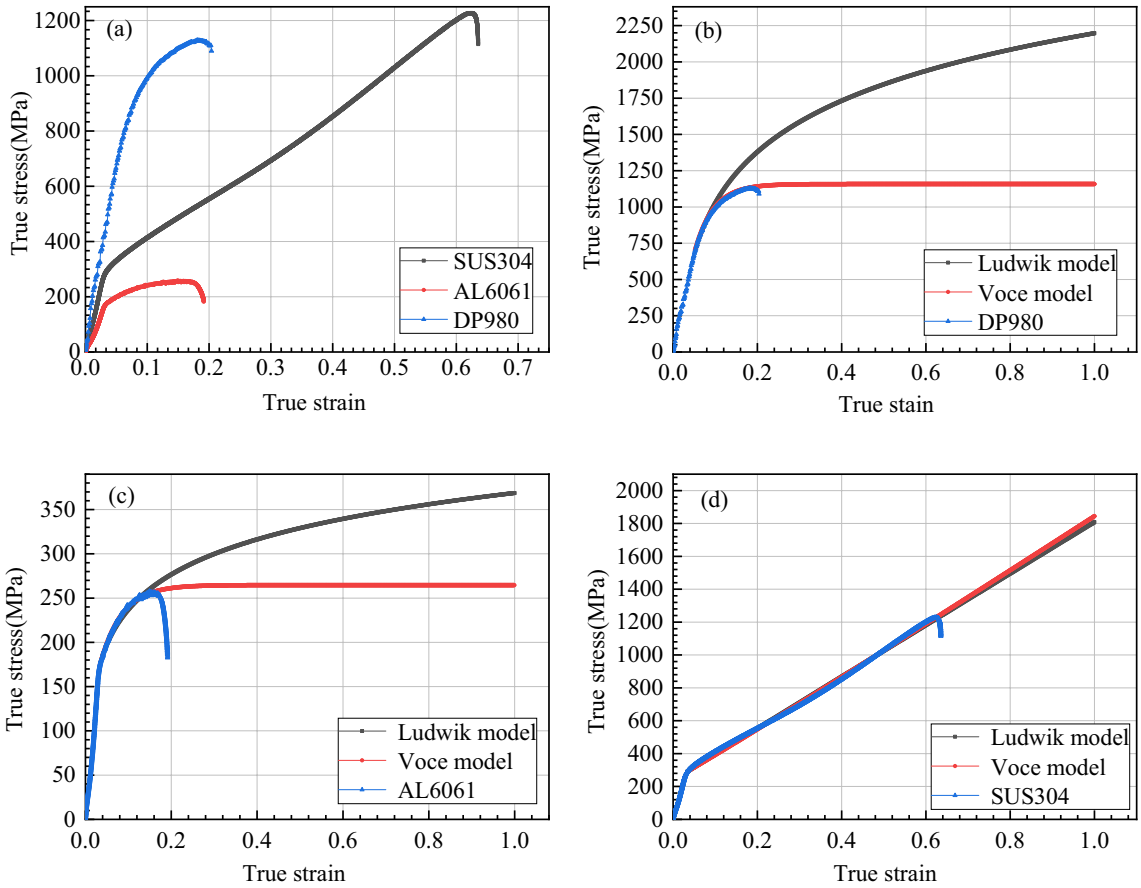

Figure 1 **a** Stress-strain curve, **b** DP980 stress-strain curve and the curves fitted by Ludwik and Voce model, **c** AL6061 stress-strain curve and the curves fitted by Ludwik and Voce model; **d** SUS304 stress-strain curve and the curves fitted by Ludwik and Voce model

$$\sigma = \begin{cases} E\varepsilon, & \varepsilon \le \varepsilon_s, \\ \sigma_s + \alpha K\left(\varepsilon^n - \varepsilon_s^n\right) + (1-\alpha)A[\exp(-B\varepsilon_s) - \exp(-B\varepsilon)], & \varepsilon \ge \varepsilon_s. \end{cases} \tag{3}$$

When $\alpha = 1$ and $\alpha = 0$, the combination function degenerates to elementary Eqs. (1) and (2), respectively. When $\alpha \in (0,1)$, the combination function can describe hardening behavior of diverse materials precisely. The parameter identification performance of different hardening models for various materials will be analyzed later.

2.2 Flexible Prediction Model in Loading Process

The combination constitutive model has been determined above. It is necessary to give the corresponding analytical model for the hardening model. In the forming process, as the bending stroke of the punch increases, the bending angle of the sheet gradually increases. The mechanical model is shown in Figure 2.

According to the mechanical model established in Figure 2, the static equilibrium equation and the geometric relationship in y direction are obtained as

$$\sum F_y = N\cos\theta + \mu N\sin\theta - \frac{P}{2} = 0, \tag{4}$$

$$N = \frac{1}{\cos\theta + \mu\sin\theta}\frac{P}{2}. \tag{5}$$

Among them, μ is the friction coefficient, θ is the rotation angle at the die fillet, P is the bending force, r_d is die radius, r_p is punch radius, N is the direct reaction force at the fulcrum, M is bending moment, l is the distance from the origin point in x direction to the tangent point of the sheet and die, L is the distance from the origin point to the center of the round corner on the die. The different mass points on curved section are in different deformation stages. ρ_x is the curvature radius on the neutral layer at x, $\rho_{\lim}$ is the limited curvature radius of elastic. When ρ_x is larger than $\rho_{\lim}$, particle which is on the section of the sheet is in the state of complete elastic deformation. When ρ_x is less than $\rho_{\lim}$, particle which is on the section of the sheet is in the state of complete elastic deformation or plastic deformation. The two state calculation methods are as follows:

1) In the process of elastic deformation, the limited curvature radius of elastic $\rho_{\lim}$ is obtained by generalized Hooke's law which is under the principal stress state:

$$\rho_{\lim} = \frac{E(1-\nu+\nu^2)^{1/2}\bar{y}}{\sigma_s(1-\nu^2)}, \tag{6}$$

where ν is Poisson's ratio, $\bar{y}$ is the ordinate value under the elastic limit.

2) In the process of elastic-plastic deformation, the deformation zone can be simplified to plane strain state, which means ε_z=0. According to the assumptions, the stress in thickness direction during the air bending process is neglected, which means σ_y=0. And the deformation zone conforms to the small deformation assumption, which means the strain distribution on the section is linear. The bending moment of the sheet is calculated by the following formula:

$$M = M_e + M_p, \tag{7}$$

where M_e is elastic bending moment, M_p is plastic bending moment.

According to the first elementary function 1 and the second elementary function 2, the combined bending moment calculation model is established as

$$\begin{aligned} M_e &= 2b\int_0^{\varepsilon_{xs}\rho_{\lim}} \frac{E}{1-\nu^2}\frac{y}{\rho_x}y\mathrm{d}y, \\ M_p &= 2b\int_{\varepsilon_{xs}\rho_{\lim}}^{t/2} \alpha\left[\frac{2}{\sqrt{3}}\left(\sigma_s - K\varepsilon_s^n\right) + \frac{2}{\sqrt{3}}K\left(\frac{2}{\sqrt{3}}\frac{y}{\rho_{\lim}}\right)^n\right]y\mathrm{d}y \\ &\quad + \int_{\varepsilon_{xs}\rho_{\lim}}^{t/2} (1-\alpha)\left[\frac{2}{\sqrt{3}}(\sigma_s + A\exp(-B\varepsilon_s)) + \frac{2}{\sqrt{3}}A\left(-\exp(-B\frac{y}{\rho_x})\right)\right]y\mathrm{d}y, \end{aligned} \tag{8}$$

where y is the ordinate value of sheet cross section, b is the width of cross section , t is the thickness of the sheet metal, when α=1, the combined model degenerates to Eq. (1); when α=0, the combined model degenerates to Eq. (2); when $\alpha \in (0,1)$, the combined model can describe diverse relationships between bending moment and curvature.

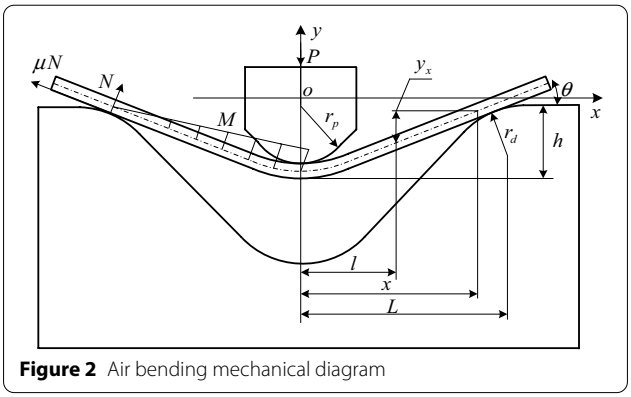

Figure 2 Air bending mechanical diagram

As the bending stroke of the punch increases, the radius of curvature under the punch gradually decreases. When the radius of curvature under the punch is $\rho_{\min}>r_p+t/2$, the area closing to the punch of the sheet did not appear, as shown in Figure 3(a); when the radius of curvature under the punch is $\rho_{\min}=r_p+t/2$, as shown in Figure 3(b), the area closing to the punch of the sheet appeared.

According to the situations whether the die is attached or not, the curvature of each point on the sheet is calculated by the following formula:

$$\rho_x = \begin{cases} r_p + t/2, \ \rho_{\min}(M) \le r_p + t/2, \\ \rho(M), \ \rho_{\min}(M) > r_p + t/2. \end{cases} \tag{9}$$

Next, these control equations are used to establish the relationship between bending force and bending stroke during loading for each deformation state. Through a trial analysis, when the die span is larger, there is no monotonous relationship between the bending force and the stroke, in other words, when the stroke is increasing, the bending force which is corresponding to the next stroke increment may be larger or smaller than the current force. In order to simplify solution, a return back algorithm is used for calculation. At first, it is assumed that the bending force is larger than the current force, then the algorithm will find the corresponding stroke. If the stroke can not be found in the forward search direction, the search direction will be adjusted backward. Until the convergence condition is meet, the algorithm exits the search program. This calculation process is shown in Figure 4.

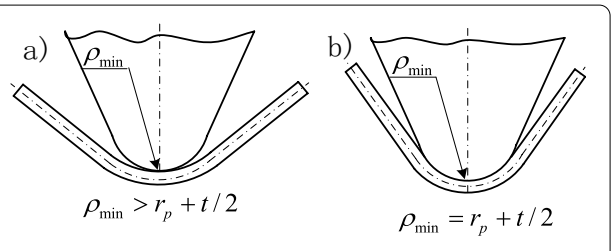

Figure 3 Contact state during forming: **a** No contact the punch; **b** Contact the punch

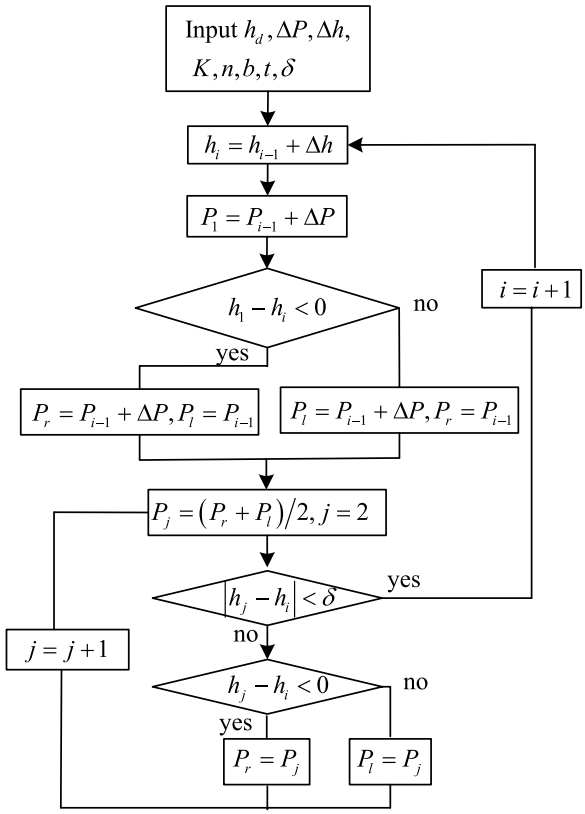

Figure 4 Program calculation process

2.3 Prediction Model in Unloading Process

The accurate descriptions of the bending loading and unloading process are important for the springback

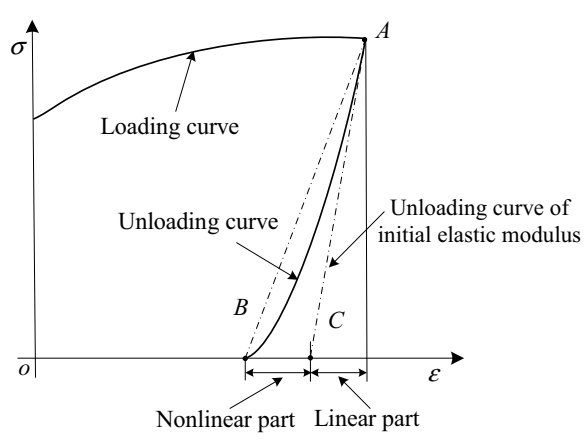

Figure 5 Stress and stain curve in unloading stage

prediction. In the elastic theory, it is assumed that the elastic unloading deformation is linear, so some high-order terms are ignored. But after certain plastic deformation occurs, these high-order terms will bring a high nonlinear effect on the unloading deformation of some materials, such as high strength steel. So in the unloading stage, the stress-strain nonlinear relationship of sheet metal is necessary to incorporate, and its typical unloading stress-strain curve is shown in Figure 5.

According to the reference, the elastic modulus is exponentially described as a function of the total strain, as shown in the following equation:

$$E_u = E_0 - (E_0 - E_a)[1 - \exp(-\xi\varepsilon)], \tag{10}$$

where E_u is elastic modulus during unloading, E_0 is initial elastic modulus, E_a is saturated modulus.

It can be concluded that under the bending moment, the relationship between the springback curvature and the bending moment is shown as follows:

$$M = 2\int_0^{t/2} E_u \frac{y^2}{\rho_x^u} b\mathrm{d}y, \tag{11}$$

where ρ_x^u is the radius of curvature at a point x after unloading the bending moment M. The amount of variation in curvature after springback can be further expressed as

$$\Delta K = \frac{M}{E_a I + (E_0 - E_a) I'} = \frac{M}{W}, \tag{12}$$

$$\frac{1}{\rho_x^u} = \frac{1}{\rho_x} - \Delta K, \tag{13}$$

where $I' = 2b\left(\frac{t^2 B}{4A} - \frac{tB}{A^2} + \frac{2B}{A^3} - \frac{2}{A^3}\right)$, $A = -\frac{\xi}{\rho_x}$, $B = \exp\frac{At}{2}$, W is bending stiffness.

2.4 Sequential Identification Strategy for Nominal Parameters

The prediction model of loading process which is based on combination elementary function and the prediction model of unloading process have been given. From above analysis, loading model and unloading model contain many parameters. Identification the nominal parameters using global optimization model usually fall into local optima, because the global optimization problem is non convex. So sub-optimization problems need to be decoupled from the global model, then the sequential identification strategy for nominal parameters needs to be determined. It is easy to obtain the full force stroke curve of the loading and unloading process from bending equipment, but different sub-optimization problems

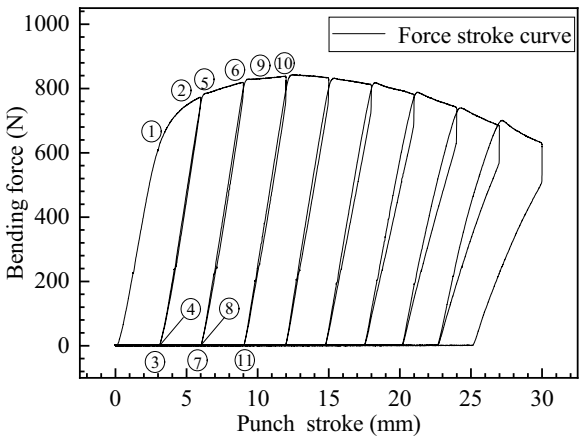

Figure 6 Force-stroke curve of repeated loading and unloading

using different segments from full load curve. So the first task is to segment the load curve for each sub-optimization problem.

The force and stroke sensors collect data from the bending machine synchronously, The original data are recorded as (h^o_i, P^o_i), i=1, 2,..., m_e. The curves of the data are shown in Figure 6. The interpolation algorithm can be used to resample the experimental data at equal intervals to solve the problem that the experimental data and the predicated data from the mechanical prediction model are unequal on the abscissa. The interpolated experimental data points are recorded as (h^e_i, P^e_i), i=1, 2,..., m_{int}. The sampling interval is Δh, and the calculation formula is presented below. The force stroke data points given by the analytical model are recorded as (h^a_i, P^a_i), i=1, 2,..., m_{int}, and m_{int} is the number of experimental data set after resampling.

$$P_j = P_i^e + \left(j\Delta h - h_i^e\right)\frac{P_{i+1}^e - P_i^e}{h_{i+1}^e - h_i^e},\ j = 1, 2, ..., m_{\text{int}},\quad i \in \{1,\ 2, ...,\ m_e\}\left|\left(h_i^e \le j\Delta h \le h_{i+1}^e\right)\right., \tag{14}$$

$$h_j = j\Delta h,\ j = 1,\ 2, ...,\ m_{\text{int}}. \tag{15}$$

Based on the above-described model, these experimental data points can be divided into four segments according to different purposes. The data points before yield bending are used to optimize the elastic modulus, and the transition points between elastic and plastic bending are used to optimize the yield strength, while the data points after yield bending are used to optimize the hardening parameters, and the unloading data points are used to optimize the variable modulus parameters. The window method [32] is used to automatically identify the

each segment boundary points of the experimental and predicated force–stroke curves. Finally, automatic curve segmentation is completed.

The boundary points for each segment on the curve can be stably extracted by moving the window. The thresholds of the abscissa and ordinate are set to Δh_c and ΔF_c, respectively. In order to keep the threshold universal, the curve data are normalized, the number of window points is determined by the following formula:

$$n_w^i = \left\{ \omega_i : \omega_i \in \{2,\ 4, \ldots,\ m_{\text{int}} - i\} \middle| \left(\begin{array}{l} \sum_{j=1}^{\omega_i} abs(h_{i+j}^{norm} - h_{i+j-1}^{norm}) \geq \Delta h_c \vee \\ \left(F_{i+j}^{norm} - F_i^{norm}\right) \geq \Delta F_c,\ j = 2,\ 4, \ldots,\ \omega_i \end{array} \right) \right\},\ i = 1,\ 2, \ldots, \tag{16}$$

where i is the index of the starting point (h_i^{norm}, F_i^{norm}) of the window data. When the length of the horizontal coordinate or the height of the vertical coordinate of the window whose end point ($h^{norm}{}_{i+j}$, $F^{norm}{}_{i+j}$) meets the conditions, $n^i{}_w+1$ is the adaptive window size which i is the index starting point. the points between $[i,\ i+n^i{}_w/2]$ and $[i+n^i{}_w/2,\ i+n^i{}_w]$ are fitted linearly respectively, $o^i{}_s$ is defined as the starting point on the straight line, $o^i{}_m$ is defined as the middle point, $o^i{}_f$ is defined as the end point, the rotation angle is calculated from crossing the two vectors, it is expressed as follows:

$$\alpha_i = -\frac{\overrightarrow{o_s^i o_m^i} \times \overrightarrow{o_m^i o_f^i}}{\left|\overrightarrow{o_s^i o_m^i} \times \overrightarrow{o_m^i o_f^i}\right|} \arccos\left(\frac{\overrightarrow{o_s^i o_m^i} \cdot \overrightarrow{o_m^i o_f^i}}{\left|\overrightarrow{o_s^i o_m^i}\right| \left|\overrightarrow{o_m^i o_f^i}\right|} \right),\ i = 1,\ 2, \ldots \tag{17}$$

If the calculated angle is positive, it means that the vector $\overrightarrow{o_s^i o_m^i}$ clockwise rotates relative to the vector $\overrightarrow{o_m^i o_f^i}$, conversely, if the angle is negative. The rotating angle at each coordinate point can be obtained, the index of the coordinate point is set as the abscissa, the angle and stroke are set as the ordinate, and the curve is shown in Figure 7 and Figure 8. It is evident from the curve that the loading and unloading of stroke curve is an isosceles triangle. It is shown from angle curve at the ath loading and unloading, there are three peak points, the points 1, 2, and 3 are shown in Figure 8. For the bth loading and unloading, point 4 is a valley point, while 5, 6, and 7 are peak points. For the cth and subsequent loading and unloading, the four boundary points are generated too. The program determines the boundary points for each cycle (a–i). Finally, the segmented force curve is shown in Figure 9.

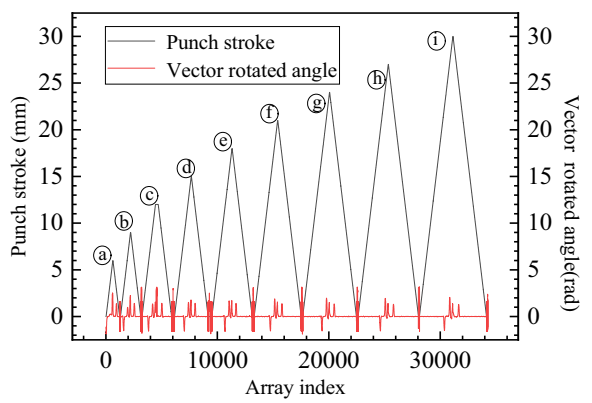

Figure 7 Loading and unloading force curve and corresponding angle curve

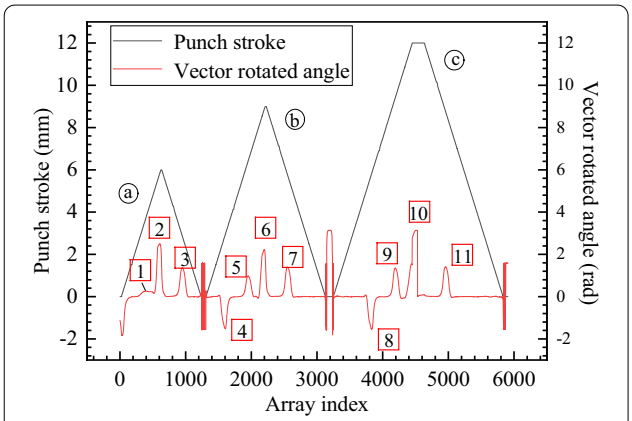

Figure 8 Enlarged view of loading and unloading force curve and corresponding angle curve

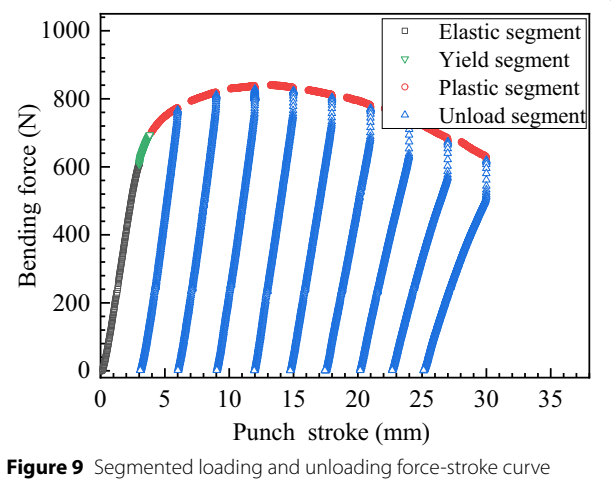

Figure 9 Segmented loading and unloading force-stroke curve

The objective functions of the elastic, yield, plastic, and elastic unloading segments are defined as follows. When the predicated and experimental data are sufficiently close, in other words, each of the objective functions takes the minimum value, the selected nominal parameters are reasonable. Now four sub-optimization problems are built. They are optimized one by one sequentially, this is a sequential identification strategy for nominal parameters.

$$G_e(X_k^e) = \frac{1}{2}\sum_{i\in\Omega_e}\frac{\left(P_i^e - P_i^a\right)^2}{i_e},\ i = 1,\ 2, ...,\ i_e, \tag{18}$$

$$G_y(X_k^y) = \frac{1}{2}\sum_{i\in\Omega_y}\frac{\left(P_i^e - P_i^a\right)^2}{i_y},\ i = 1,\ 2, ...,\ i_y, \tag{19}$$

$$G_p(X_k^p) = \frac{1}{2}\sum_{i\in\Omega_p}\frac{\left(P_i^e - P_i^a\right)^2}{i_p},\ i = 1,\ 2, ...,\ i_p, \tag{20}$$

$$G_u(X_k^u) = \frac{1}{2}\sum_{i\in\Omega_u}\frac{\left(P_i^e - P_i^a\right)^2}{i_u},\ i = 1,\ 2, ...,\ i_u. \tag{21}$$

The nominal parameter ranges for each sub-optimization problem are set as

$$\begin{cases} a_k^e \le X_k^e \le b_k^e,\ k = 1,\ 2, \cdots,\ l_e, \\ a_k^y \le X_k^y \le b_k^y,\ k = 1,\ 2, \cdots,\ l_y, \\ a_k^p \le X_k^p \le b_k^p,\ k = 1,\ 2, \cdots,\ l_p, \\ a_k^u \le X_k^u \le b_k^u,\ k = 1,\ 2, \cdots,\ l_u, \end{cases} \tag{22}$$

where l_e, l_y, l_p, l_u are the number of nominal parameters that need to be optimized, and variables $X^e{}_k$, $X^y{}_k$, $X^p{}_k$, $X^u{}_k$ are the degree of freedom. For each sub-optimization problem, a quadratic approximation function is used for each objective function. At the kth iteration, there is an approximate function shown as follows:

$$Q_k(\boldsymbol{Y}_j) = G_s(\boldsymbol{Y}_j),\ j = 1,\ 2,\ 3, \cdots,\ m, \tag{23}$$

where $m\in[(l_s+2),\ (l_s+1)(l_s+2)/2]$, $s\in\{e, y, p, u\}$. The optimization problems of above four objective functions are transformed into the minimizing problems of approximate functions. A optimization problem is shown as follows:

$$\begin{aligned} &\min\ Q_k(\boldsymbol{X}_k + \boldsymbol{d}), \\ &\text{s.t. } \boldsymbol{a} \le \boldsymbol{X}_k + \boldsymbol{d} \le \boldsymbol{b}, |\boldsymbol{d}|_2 \le \Delta_k, \\ &\boldsymbol{X}_k \in \{\boldsymbol{Y}_j : j = 1,\ 2, \ldots, m\} \big| \min\left\{G_s(\boldsymbol{Y}_j) : j = 1,\ 2, \ldots, m\right\}, \end{aligned} \tag{24}$$

where $\boldsymbol{d}$ is the vector step of each iteration and Δ_k is the confidence radius at the kth iteration.

3 Feedback Model Using Online Data

The deformation control accuracy is affected by some assumptions introduced, mold misaligned and wear, so online closed-loop feedback mechanism is necessary. In the closed-loop bending control model, the target bending angle after springback is defined as α_{obj}, the bending angle after springback in the last forming is defined as α_{i-1}, then the deviation angle of the previous forming is e_{i-1}, and it is expressed as

$$e_{i-1} = \alpha_{obj} - \alpha_{i-1}. \tag{25}$$

There is a assumed nonlinear relationship between the bending stroke and bending angle after springback over a wide range. The spingback angle can be approximated by a linear relationship in a small neighbourhood of the nominal reference point h_0, and the first-order Taylor is represented as

$$\alpha = \alpha_0 + \left.\frac{\partial\alpha}{\partial h}\right|_{h=h_0}(h - h_0). \tag{26}$$

According to Eq. (26), the relationship between the current forming deviation and the stroke increment is

$$\Delta h_i^p = K_c e_i, \tag{27}$$

where K_c is the control coefficient, the plastic bending stroke of the ith bending is

$$h_i^p = \Delta h_i^p + h_{i-1}^p. \tag{28}$$

The total plastic bending stroke of the ith bending is

$$h_i = h_i^p + h^e. \tag{29}$$

The bending angle after springback of the ith forming is

$$\alpha_i = K_b(h_i - h_e), \tag{30}$$

where K_b is the linear coefficient of bending model. The difference equations of the discrete control system are Eqs. (25)–(29), z-transformation is performed on the above-stated difference equation to obtain the transfer function, and the stability of the system is analyzed using these transfer functions. The transformed equations are as follows:

$$e(z) = \left(\alpha_{obj}(z) - \alpha(z)\right)z^{-1}, \tag{31}$$

$$\Delta h^p(z) = K_c e(z), \tag{32}$$

$$h^p(z) = \Delta h^p(z) + h^p(z)z^{-1}. \tag{33}$$

The relationship between bending stroke and the stroke increment obtained from an integral element, as well as the transfer function of Eq. (30) are described as

$$\frac{h^p(z)}{\Delta h^p(z)} = \frac{1}{1-z^{-1}}, \tag{34}$$

$$\alpha(z) = K_b h^p(z). \tag{35}$$

Eqs. (31)–(35) can be used to get the transfer function of the closed-loop feedback control system as

$$\frac{\alpha(z)}{\alpha_{obj}(z)} = \frac{K_c K_b}{z-1+K_c K_b}. \tag{36}$$

The characteristic equation of the system is

$$z-1+K_c K_b = 0. \tag{37}$$

According to Eq. (37), the characteristic root of the system can be obtained as

$$z = 1-K_c K_b. \tag{38}$$

In the z-plane, the system satisfies the stability condition as

$$|1-K_c K_b| \le 1. \tag{39}$$

The transfer function of control variable is shown as follows:

$$\frac{h^p(z)}{e(z)} = \frac{K_c}{z-1}. \tag{40}$$

Inverse z-transformation of Eq. (40), the difference equation used for the controller is

$$h_i^p = K_c e_{i-1} + h_{i-1}^p, h_0^p = h^e. \tag{41}$$

According to the stability condition, when $0 \le K_c \le 2/K_b$, the closed-loop system converges steadily, different values of K_c are selected, the output results of the system are shown in Figure 10. When the target bending angle of the springback control system is altered from 0° to 20°, that is increased by 20°, and K_c=2/K_b(PT 20-2/K_b), the output of the system is an oscillation curve with the same amplitude. When K_c=1.5/K_b(PT 20-1.5/K_b), some overshoots occur in the early stages of the system. After five adjustments, the output of the system meets the control requirement. When K_c=0.9/K_b(PT 20-0.9/K_b), the system converges to the steady-state value after one time. When K_c=0.5/K_b(PT 20-0.5/K_b), the system output is a rising asymptotic curve, and after five adjustments, the output of the system reaches the control requirement. When the target bending angle is altered from 40° to 20°, that is reduced by 20°, the output curve of the system with an angle increased by 20° is symmetrical to that with an angle reduced by 20°. Figure 11 shows the output of target bending angle 60°. It is evident that when the target bending angle increases, so do the oscillation and overshoot amplitude.

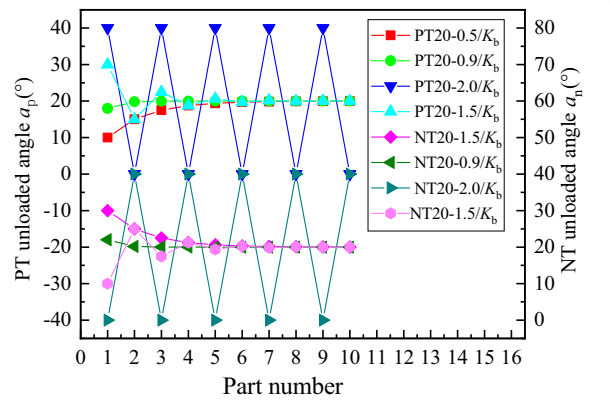

Figure 10 Curves of bending angle after springback

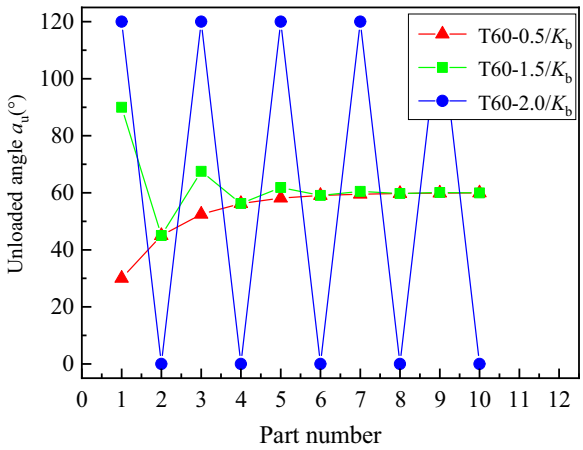

Figure 11 Curves of bending angle after springback

According to the above-stated analysis, when $\alpha^i_{uo} > \alpha^{i-1}_{uo}$, a positive step is produced, and when $\alpha^i_{uo} < \alpha^{i-1}_{uo}$, a negative step is generated. For the positive step signal, when the output of the system overshoots, the system will produce an over-bending phenomenon, which is irreparable and generates unqualified parts. When the output of the system is a gradual line, then multiple forming can be used for correction, however, too many corrections will reduce production efficiency. Negative step signals are contrary to positive ones, and the maximum overshooting value results in under-bending. Meanwhile, considering that the material properties of different batches and directions exhibit obvious fluctuations, system parameters with a certain safety margin are given to ensure that they are always under-bending during the

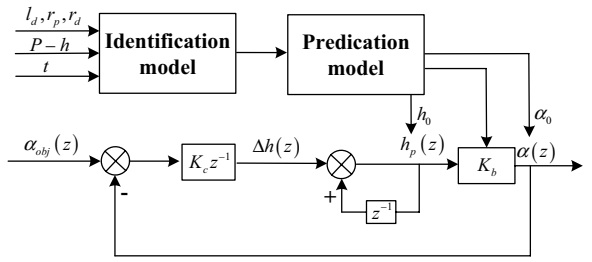

Figure 12 Control system flow chart

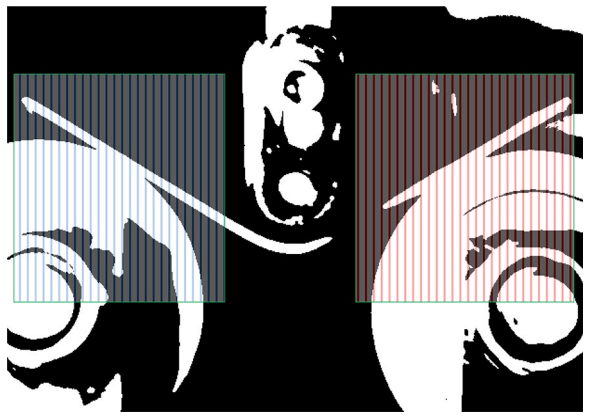

Figure 13 Measurement image to obtain unloaded angle

adjustment process. The parameters of the system controller are set to

$$K_c = \begin{cases} (1-\beta)\Big/K_b,\ \alpha_{uo}^{i} > \alpha_{uo}^{i-1}, \\ (1+\beta)\Big/K_b,\ \alpha_{uo}^{i} < \alpha_{uo}^{i-1}, \end{cases} \tag{42}$$

where β is safety margin for sheet metal fluctuations.

4 Control Strategy of Flexible Control System

Flexible prediction model and sequential identification strategy are built separately. The control flow chart is shown in Figure 12. When the flexible system is used to bend a kind sheet metal for the first time, the system identifies the nominal parameters of the prediction model using sequential identification strategy automatically. The prediction model completes adjustment of the system working point. After the system arrives at the vicinity of the working point, the feedback correction model participates in compensation, and thereafter, interference and deviation are eliminated near the working point. The control strategy of the flexible system is determined. When the system is adjusted in a large range, the nominal working point of the system is found by optimal model. When the nominal working point fluctuates in a small range, the system control accuracy is compensated by the data model. These promote flexibility and efficiency of the control algorithm for the air bending process.

5 Flexible Control Experiment System

5.1 Angle Measurement after Springback

To improve the accuracy and efficiency of angle measurement, a camera is used for online measurement. The grids shown in Figure 13 are created on the left-hand and right-hand sides of the image. The corresponding pixel coordinates are extracted at the abrupt pixel edge. The pixel coordinates extracted from the left-hand and right-hand grid areas are linearly fitted by the least squares method to obtain the line equations, and the bending angle of the part is determined. Integrating the image processing algorithm into the computer control system program, the result is shown in Figure 13.

In order to verify the measurement accuracy of the online image measurement method used in this paper, the 3000iTM series of flexible three-coordinate measurement system produced by CimCore is used. Using PowerINSPECTTM measurement software and three-coordinate measuring tools to perform point-contact detection on the bending angle after unloading, the deviation is 0.01%. The image method used in this paper can meet the needs of experiments and engineering.

5.2 Flexible Control Experiment System and Softwares

In this study, a free V-bending flexible control experimental system is developed. The execution unit of the experimental system utilizes a servo electric cylinder, and a Delta 1.5 kW servo motor is used as the power source. The reduction ratio of the reducer is 1:12, and the screw lead is 10 mm. A grating ruler with an accuracy of 1 μm is installed on the movable beam of the machine, which form a fully closed-loop system with a servo drive. A control software is developed in the industrial control computer IPC-610H. The pulse control cards, pulse acquisition counting cards, and voltage acquisition cards are all connected through the PCI bus. The pulse control card is used for pulse generation to control the servo motor, while the pulse acquisition card is used for counting the pulse signal of the grating ruler, and the voltage acquisition card is used for the force sensor. The control software is written in the G programming language of LabVIEW. The software and hardware structures are shown in Figure 14. The mechanical system for air bending experiment is shown in Figure 15.

The control process of this study has been built into the computer program. When the geometric parameters of the material are adjusted in the interface, the program

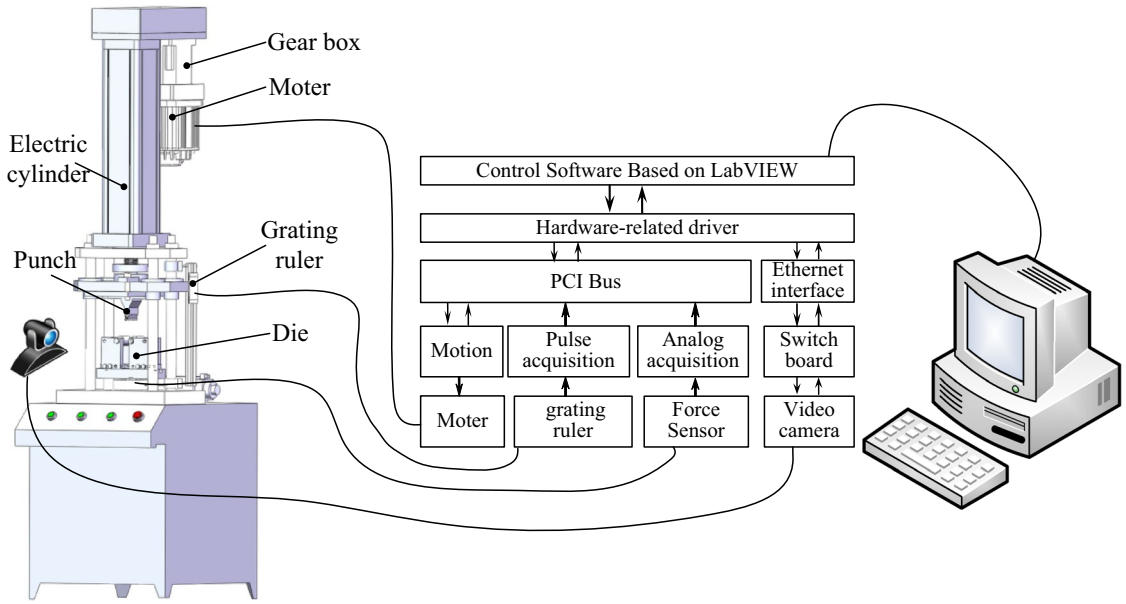

Figure 14 Hardware and interface composition of control system

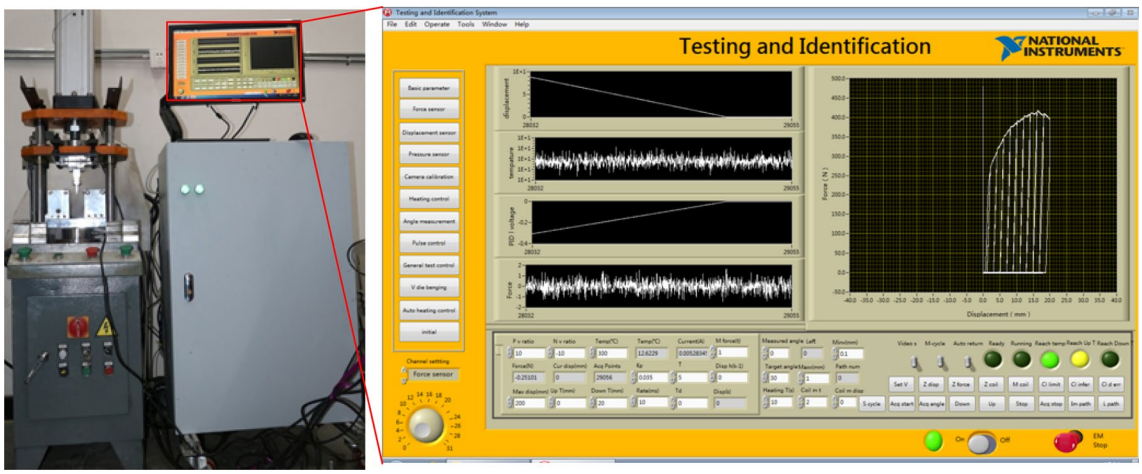

Figure 15 The mechanical system for air bending experiment

will identify the parameters automatically. The control accuracy of the experimental system controlled by computer is affected by various interference. In order to eliminate the above interference, after the identification is completed, the system enables the feedback control algorithm to correct the deviation.

5.3 Results of Online Flexible Control System

To confirm the accuracy of the above-mentioned method, high-strength steel sheets DP980, 304 stainless steel, ST12, and 6061 aluminum alloy were used in the verification experiment. The thickness of the DP980 sheet, 304 stainless sheet, ST12 sheet, and 6061 sheet were 2.2 mm, 0.8 mm, 1.0 mm, and 2.0 mm, respectively. A set of moulds was used to conduct an experimental study on the springback control of air bending.

In this study, the material parameters self-identification optimization algorithm needs to explicitly provide the coefficient feasible ranges of the two constitutive models. The parameter ranges of these two models are determinable by fitting, where the parameter ranges of the Voce model are $E \in [10000, 300000]$, $\sigma_s \in [100, 1400]$, $A \in [10,$

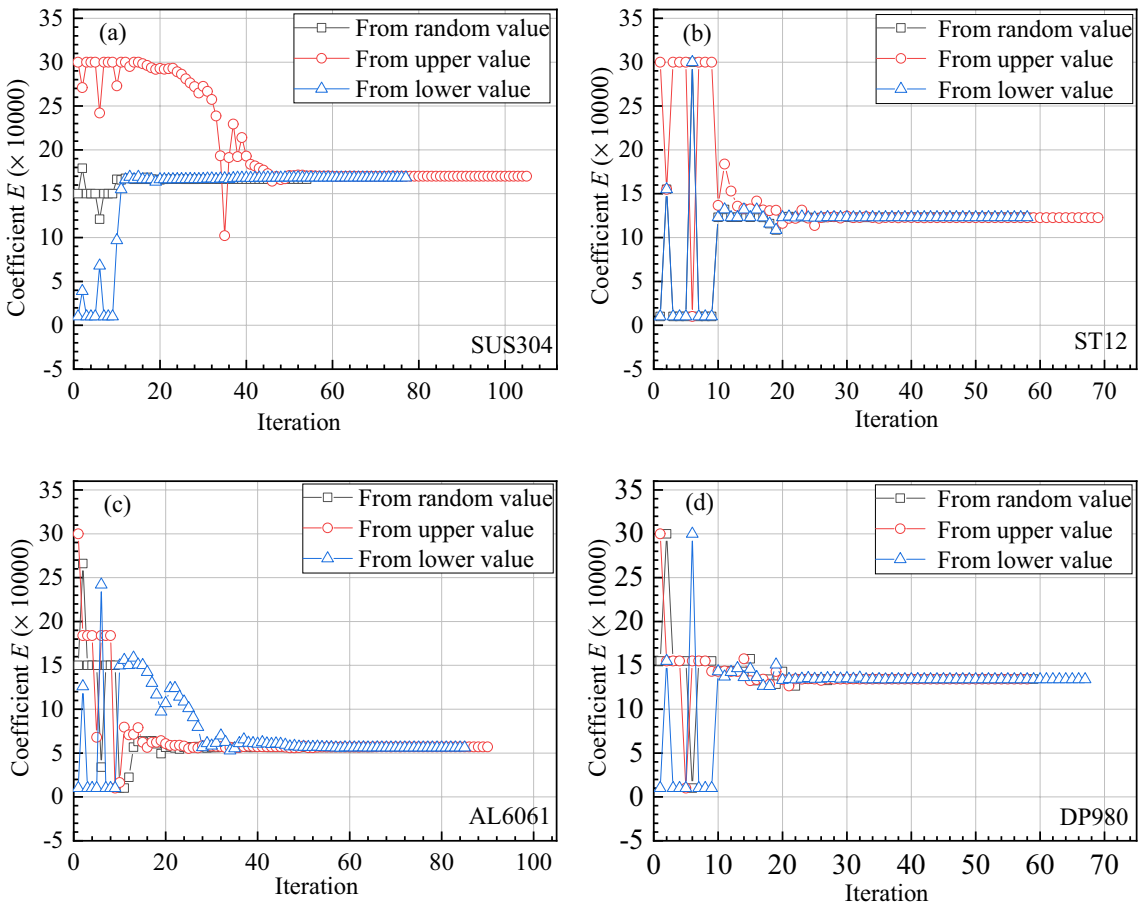

Figure 16 The learning processes of elastic modulus: **a** SUS304; **b** ST12; **c** AL6061; **d** DP980

2000] and $B \in [5, 200]$. In the Ludwik model, the elastic modulus and the yield strength range are same, and the ranges of the parameters K and n are $K \in [10, 5000]$ and $n \in [0.001, 1]$, respectively. To verify the convergence of the algorithm, each parameter was optimized with three different initial values within the feasible range. The selection principle of the three initial values are that a point nears the upper boundary and another nears the lower boundary, and a random point is picked within the feasible range. The identification results of the elastic modulus of SUS304, ST12, AL6061, and DP980 are shown in Figure 16.

It is evident from the figure that the elastic modulus is relatively stable during the iterative process, and the optimal approximate surface is constructed by several function value calculations in the trust region that rapidly converges to the target value through approximately 30 iterations. Although the elastic modulus of the four materials is different, the algorithm can always converge to a fixed value. The elastic modulus parameters, the length of the elastic phase, and the number of experimental points collected at a fixed acquisition frequency are different, which affect the calculation of the target function, and consequently influence the convergence efficiency of the elastic modulus, but not affect the convergence results. The yield strength parameter identification process is shown in Figure 17.

Figure 17 apparently reveals that the SUS304, ST12, and Al6061 materials enter into the fast convergence stage after ten iterations. Furthermore, after approximately 60 iterations, their yield strength enter a stable convergence stage. The yield strength of AL6061 has a certain fluctuation, which is smaller than the yield strength of DP980. The total number of iterations of AL6061 materials is less than that of the other three materials, which have equivalent total iteration numbers. By comparing the four force–stroke curves, the DP980 transition from linear to nonlinear is longer, and the identification efficiency is relatively lower. The yield strength of the four materials converged to a fixed value after approximately 130 iterations. The identification processes of the SUS304 and ST12 materials are shown in Figure 18.

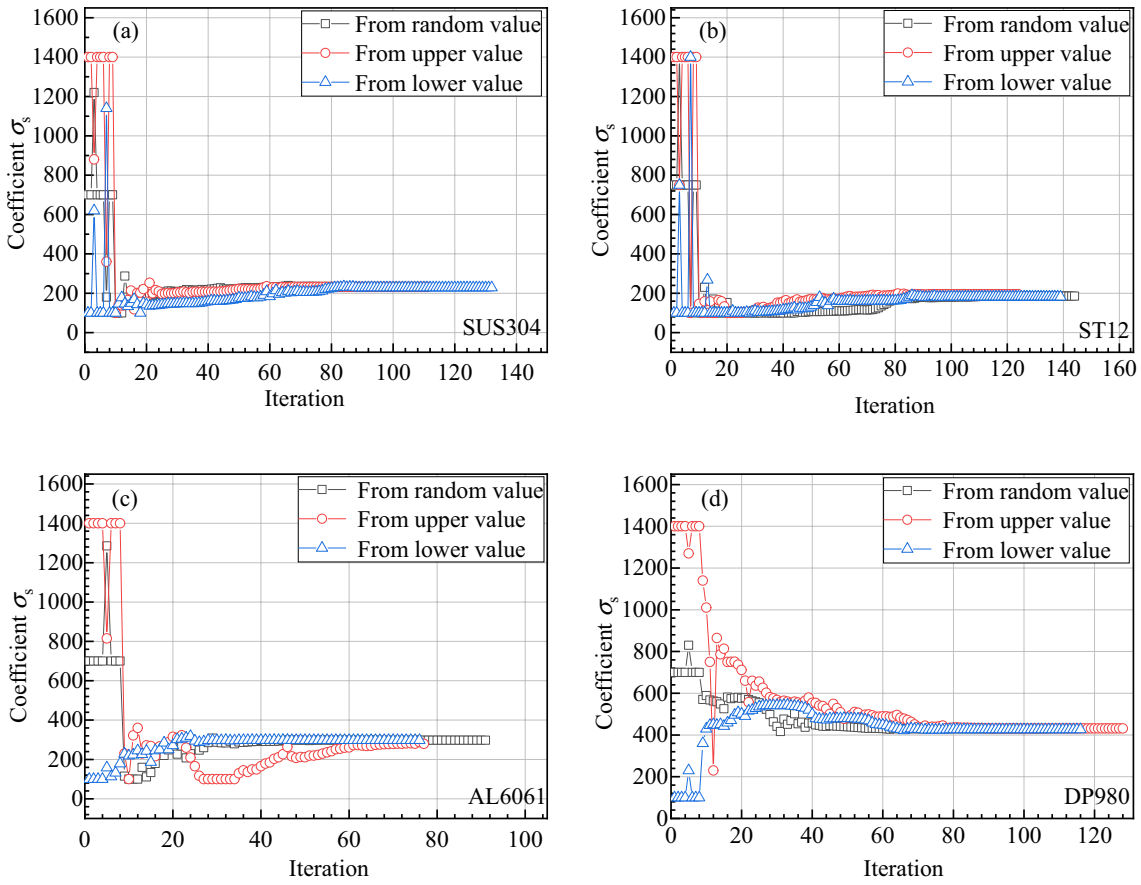

Figure 17 The learning processes of material yielding: **a** SUS304, **b** ST12, **c** AL6061, **d** DP980

In the Ludwik model, there are two parameters that comprehensively control the hardening behavior of the material. Therefore, when choosing the initial value, K and n can be selected near the upper boundary, lower boundary or the middle. K and n fluctuates lightly in the early stage, and the subsequent learning process is stable.

By comparing the optimization processes of the two materials, for the initial value from the upper boundary, the SUS304 and ST12 materials converge approximately 240 and 160 iterations, respectively. In the case of the initial value from the lower boundary, both of the SUS304 and ST12 materials converge approximately 400 iterations, so the stop iterations of the initial value from the upper boundary are less than those from the lower boundary. For the Ludwik model, the initial value of the flexible system learning algorithm is recommended near the upper boundary for improving learning efficiency. Compared with the Ludwik model, the Voce model has a better saturation capacity and rapid hardening capacity in a shorter strain range. When the material hardens violently, the Voce model is preferred to describe the constitutive behavior of materials. The processes for identifying AL6061 and DP980 are shown in Figure 19.

There are two parameters in the Voce model that comprehensively control the hardening behavior of the material. It is evident from the formula that when the value of A is larger, the material hardens faster, whereas when the value of B is higher, the material saturates more rapidly, the material hardening rate is too high for larger A and B, but it is inconsistent with conventional materials. Therefore, when identifying the parameters of the Voce model, the value of parameter A is taken from the upper boundary, while that of parameter B is obtained from the lower boundary. in Figure 19, the case that parameters A and B are obtained from the upper and lower boundaries is compared with the other case that parameters B and A are got from the upper and lower boundaries, the total number of iterations of the former (300) is exceeds that of the latter (200). For the Voce model, the flexible system learning algorithm selects the initial value of parameters A and B near the upper and lower boundaries, respectively, to improve the learning efficiency.

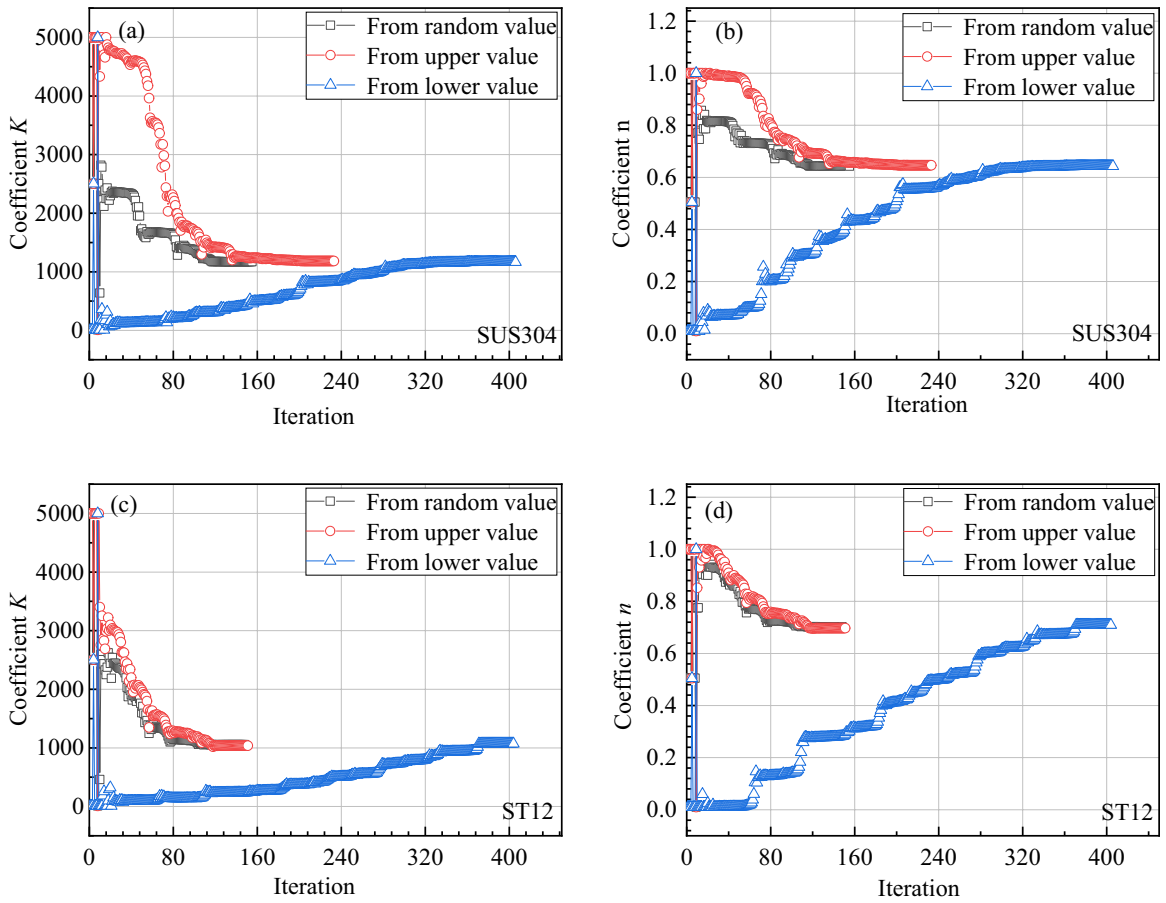

Figure 18 Learning process of Ludwik hardening parameters: **a** Parameter *K* of SUS304, **b** Parameter *n* of SUS304, **c** Parameter *K* of ST12, **d** Parameter *n* of ST12

The above-stated recognition results are summarized in Tables 1, 2.

After the optimization of elasticity, yield, plasticity, and repeated unloading, the force–stroke curves of SUS304, AL6061, ST12, and DP980 are shown in Figure 20. It is evident from the figure that the bending load slightly decreases when the punch stops, that is, the sheet bending process exhibits a certain stress relaxation phenomenon. Among them, SUS304 and AL6061 sheets show a similar decline, while the DP980 sheet exhibit the greatest decline. During reverse unloading, a slight increase in the load. The phenomenon of stress relaxation affects the force-stroke curve for unloading bending. The starting point on the force-stroke curve for unloading bending coincides with the end point of the stress relaxation. The force-stroke curve for unloading bending has a different nonlinearity degree, among which DP980 has the largest nonlinearity degree. Figure 20(a), (b), and (c) reveal that the amount of springback deformation increases with the deformation, and the established variable modulus model has a higher prediction accuracy for springback. However, the nonlinearity of the springback of the DP980 sheet increases highly compared with the other three sheets, so the deviation of the springback prediction via the variable modulus model also increases. Established prediction models have unmodeled deviations, which need to be eliminated by the online feedback algorithm.

The optimization model can quickly find the nominal work point of the flexible system, but it cannot completely eliminate the effects of online interference. Therefore, it is necessary to introduce online methods to eliminate deviations. In order to compare the closed-loop control effect, the open-loop control is also studied through one by one forming. Fluctuations were considered by cutting test specimens in the 0° and 90° directions of the sheet. To fully verify the correctness and the effect

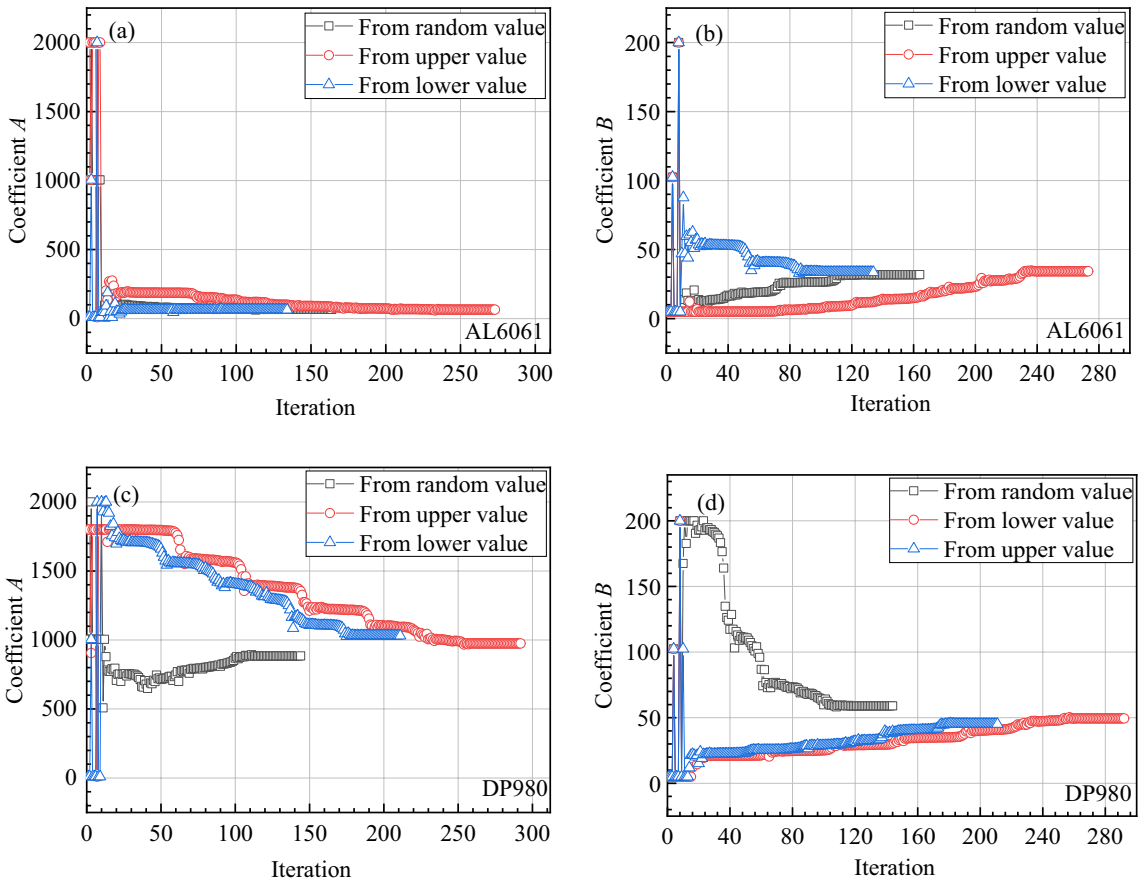

Figure 19 Learning process of Voce's hardening parameters: **a** Parameter *A* of AL6061, **b** Parameter *B* of AL6061, **c** Parameter *A* of DP980, **d** Parameter *B* of DP980

Table 1 Geometry parameters for the moulds

R_d (mm)	R_p (mm)	L (mm)	b (mm)
15	5	70	35

of the algorithm, three kinds of bending parts are to be formed. The target bending angles are 20°, 40°, and 60°. To determine the adaptive capacity of the system in the experiment, ten specimens were tracked.

For considering fluctuation of sheet property, specimens 1–3 and specimens 7–10 used blanks along the 0° direction, whereas specimens 4–6 utilized blanks along the 90° direction, and then, the adaptability of the system was evaluated. The parts were labeled after the experiment, the experimental data obtained are shown in Figure 21(a), bending parts for material SUS304 are shown in Figure 22.

Four groups experiments were conducted for each material: negative step feedback control experiment (G1-60-20), negative step no feedback control experiment

Table 2 Nominal identified material properties for different materials

Labels	σ_s (MPa)	α	E (GPa)	K	n	A	B	E_a (GPa)	ζ
SUS304	242	1	162.296	1172.889	0.64319	–	–	110.380	20.119
ST12	171	1	121.180	1054.214	0.70249	–	–	98.792	18.253
AL6061	293	0	5.7191	–	–	66.24	31.78	4.831	17.131
DP980	430	0	141.493	–	–	884	58.98	100.253	33.264

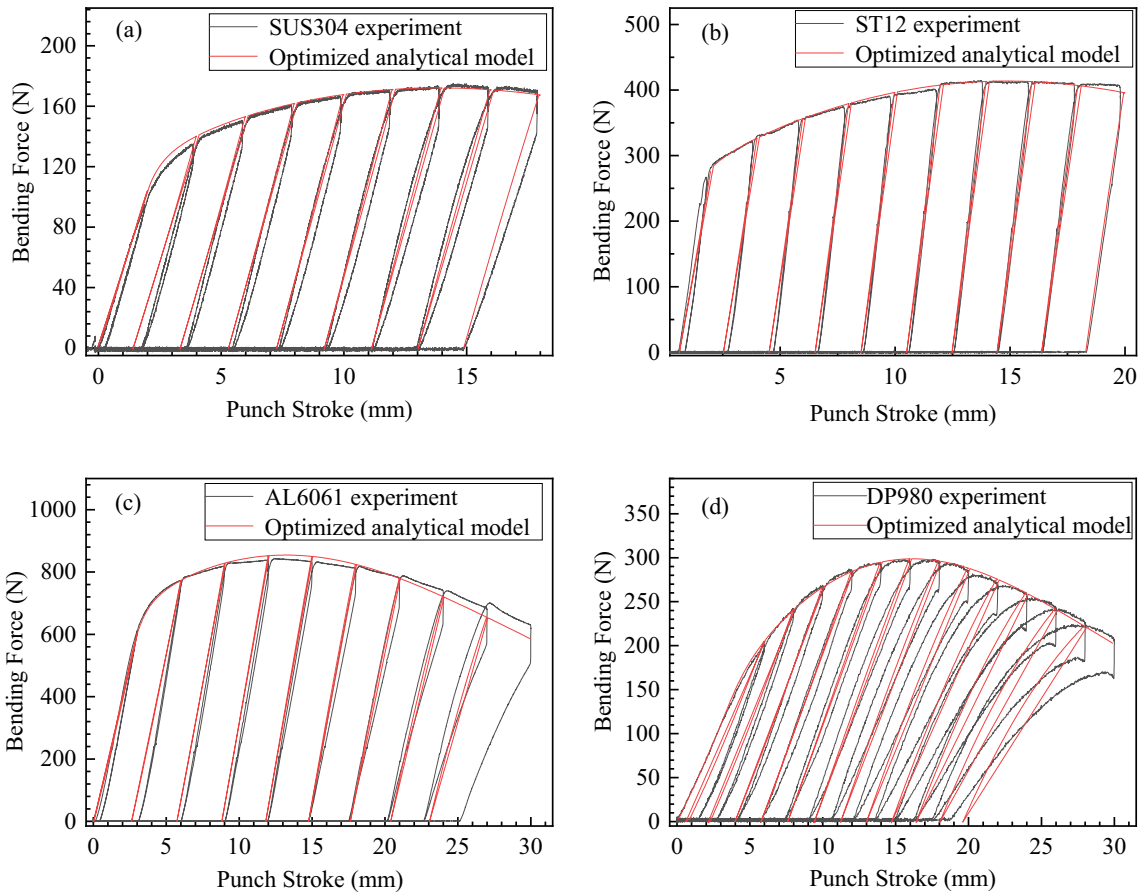

Figure 20 Comparison of the calibrated loading force stroke curve with experimental results: **a** SUS304, **b** ST12, **c** AL6061, **d** DP980

(G2-60-20), positive step feedback control experiment (G3-40-60), and positive step no feedback control experiment (G4-40-60). For each kind of four materials, it is apparent that if the flexible system is controlled with no feedback, there is always a deviation. For feedback control experiment, the bending angle of part number 1 after springback exceeds tolerance band, the bending angle of part number 2 corrected, the deviation is reduced. It can be concluded that the system has the ability to feedback out of tolerance. The results obtained through part number 1 and 2 experiments can converge quickly. The fluctuation also persists for blanks along the 0° direction from part number 1–3. Compare with part number 3 which is cut from 0° direction, part number 4 which is cut from 90° direction has a step interference caused by difference roll direction, the system can further resist this step interference.

To analyze the respond of the system to target angle step, step tests were conducted on the forming experiments of the four kinds sheets. For group 1, target angle of part number 6 is 60°, while target angle of part number 7 is 20°, so a 60°–20° negative step was occurred. In the same way, for group 3, a 40°–60° positive step was occurred. There were out-of-tolerance phenomena at the steps. To prevent the over-bending, the control parameter safety margin β was set to 10%. It can be seen from the curve that the feedback control model has a better control effect.

Furthermore, it is noticeable from the forming experiments of the four materials, materials ST12, AL6061, and SUS304 have approximately the same deviation after stabilization. However, DP980 has high-strength and large springback values, and the initial deviation of the analytical control model is larger, which implies that using online feedback methods is a better choice to eliminate deviation.

6 Conclusions

In order to precisely and efficiently form bending parts with various shapes and types, as well as small batches, a new control strategy of the flexible system is obtained.

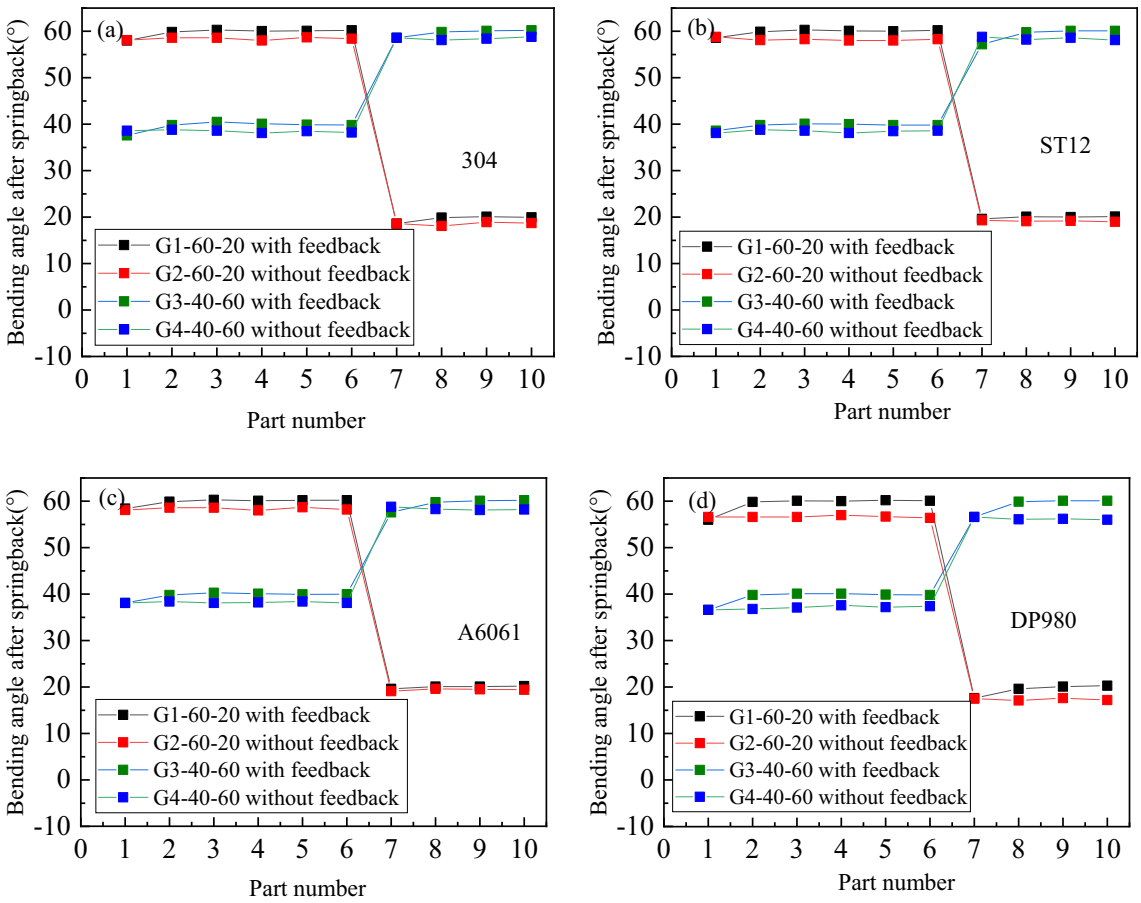

Figure 21 Curves of bending angle after springback: **a** SUS304, **b** ST12, **c** AL6061, **d** DP980

(1) In this new control system, novel prediction models are establish to ensure the applicability in diverse materials. The springback analytical model is built and incorporated the variable modulus function, a sequential identification strategy is proposed to search nominal material properties using the four sub-optimization models. A data-based feedback model is established to prevent over-bending and eliminate online deviation. Above models are merged into the new precision and flexible control strategy.

(2) In feedback model, the coefficient K_c is determined by Eq. (41) to prevent over-compensation. when $\alpha^{i}_{uo} > \alpha^{i-1}_{uo}$, the input signal of the system is a positive step signal, and when $\alpha^{i}_{uo} < \alpha^{i-1}_{uo}$, the input signal of the system is a negative step signal. Feedback model parameters with a certain safety margin β are given to ensure that part is not over-bending for positive step signal and negative step signal respectively. β is set to 10% that can meet the online requirement.

(3) In optimization models, compared with four kinds sheet metals, the allowable ranges for variables are determined for a good convergence. When choosing the initial value in the Ludwik model for optimization, K and n can be selected from the upper and lower boundaries at the same time or randomly selected from the middle. Moreover, in selecting the initial value in the Voce model for optimization. When parameters A and B are initialized from the upper and lower boundaries, respectively, the models converge easily.

(4) In the experiment of control strategy, when the desired bending angles were separately set to 20°, 40°, and 60°. For each angle, the system firstly uses sub-optimization models to search nominal point which is near to target point, secondly the system further uses feedback model to eliminate residual error between nominal point and target point. Forty parts were tracked for each kind material. The adaptive bending system converged after one iteration, and exhibited better performances.

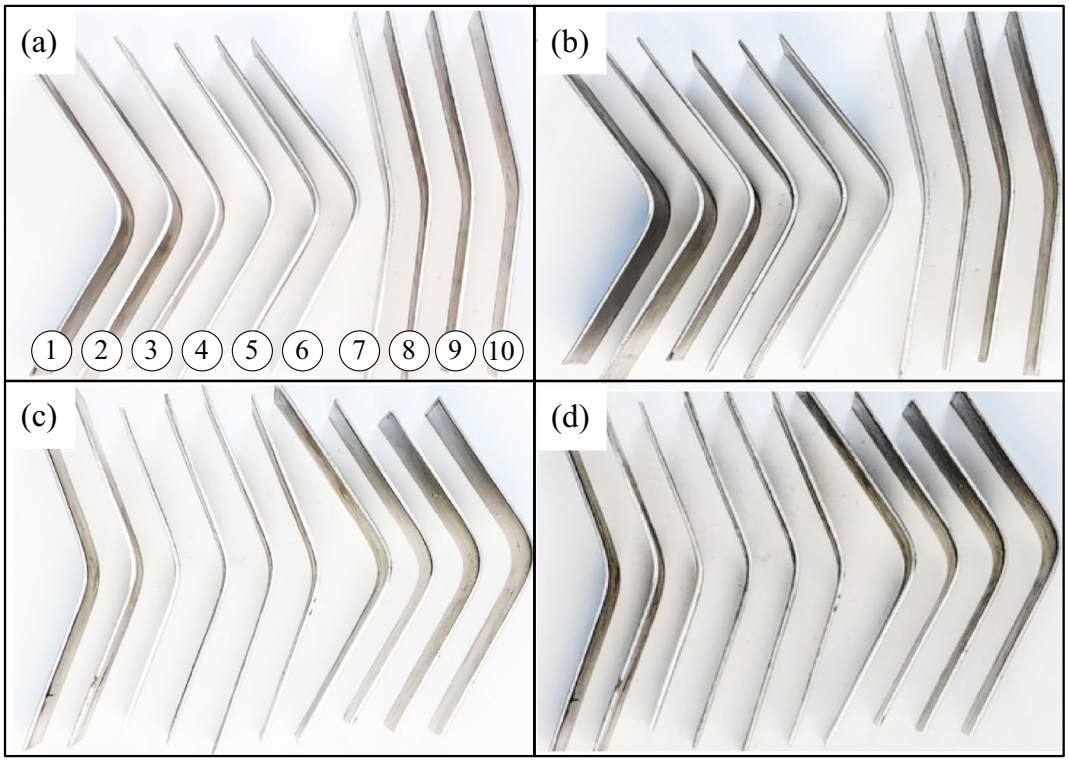

Figure 22 SUS304 bending parts after springback: **a** G1-60-20, **b** G2-60-20, **c** G3-40-60, **d** G4-40-60

Acknowledgements
Not applicable.

Author contributions
FZ was in charge of the whole trial; and YD built the software; YD and LT wrote the manuscript; YL and HQ assisted with sampling and laboratory analyses; LY and YG put forward suggestions for modification; YD, FZ and YG provided project administration. All authors read and approved the final manuscript.

Authors' Information
Yongchuan Duan, born in 1983, is currently an associate professor at *Yanshan University, China*. He received his PhD degree from *Yanshan University, China*, in 2014. His research interests include fatigue life prediction of cast aluminum alloy, and hot stamping of high strength steel plat. Tel: +86-13230309697; E-mail: yongchuan.duan@ysu.edu.cn.
Le Tian, born in 1993, obtained his master's degree from *Yanshan University, China,* in 2020. His research interests include free temperature bending forming and springback control of high strength steel plate. E-mail: wolfganglele@gmail.com.
Fangfang Zhang, born in 1984, is currently a lecturer at *Yanshan University, China*. She received her PhD degree from *Yanshan University, China*, in 2014. Her research interests include damage model establishment and optimization identification of composite materials based on multi-dimensional information; simulation of continuous friction and wear process of heterogeneous fabric liner for self-lubricating plain bearing. Tel: +86-13223387868; E-mail: fangfang.zhang@ysu.edu.cn.
Yu Liu, born in 1997, is a postgraduate student at *Yanshan University, China*. His research interests include multi-scale fracture mechanism and prediction model of high strength steel. Tel: +86-15538204689; E-mail: 15538204689@163.com.
Haidi Qiao, born in 1995, obtained his master's degree from *Yanshan University, China*, in 2021. His research interests include material property parameter identification and springback prediction. E-mail: qiao741380857@163.com.
Liu Yang, born in 1988, is currently a laboratory technician at *Yanshan University, China*. He received his PhD degree from *Yanshan University, China*, in 2021. Tel: 15369682119; E-mail: yangliu@ysu.edu.cn.
Yingping Guan, born in 1963, is currently a professor at *Yanshan University, China*. He received his PhD degree from *Yanshan University, China*, in 2004. His research interests include hot stamping forming mechanism and technology of high strength steel, forging and control of aluminum alloy wheels for high-end cars and process control technology of magnesium alloy sheet deep drawing. E-mail: gyp@ysu.edu.cn.

Funding
Supported by Natural Science Foundation of Hebei Province Iron and Steel Joint Research Fund (Grant No. E2021203163), Hebei Provincial Natural Science Foundation of China (Grant No. E2021203210).

Competing Interests
The authors declare no competing financial interests.

Author Details
[1]Key Laboratory of Advanced Forming & Stamping Technology and Science, Ministry of Education of China, Yanshan University, Qinhuangdao 066004, China. [2]College of Mechanical Engineering, Yanshan University, Qinhuangdao 066004, China.

Received: 27 November 2020 Revised: 16 August 2021 Accepted: 22 April 2022
Published online: 12 August 2022

References

[1] V Vorkov, A T García, J R Duflou. Bending parameters in heat assisted air bending of high strength steels. *Procedia Manufacturing*, 2020, 47: 1314-1318. https://doi.org/10.1016/j.promfg.2020.04.250.

[2] Asghar Zajkani, Hamid Hajbarati. An analytical modeling for spring-back prediction during U-bending process of advanced high-strength steels based on anisotropic nonlinear kinematic hardening model. *The International Journal of Advanced Manufacturing Technology*, 2017, 90(1-4), https://doi.org/10.1007/s00170-016-9387-5.

[3] W Jian, A Jl, A Cf, et al. Study on influencing factors of bending spring-back for metal fiber laminates. *Composite Structures*, 2021, https://doi.org/10.1016/J.COMPSTRUCT.2021.113558.

[4] A Pradeau, S Thuillier, J W Yoon. Prediction of failure in bending of an aluminium sheet alloy. *International Journal of Mechanical Sciences*, 2016, 119: 23-35. https://doi.org/10.1016/j.ijmecsci.2016.09.033.

[5] J Allwood, S Duncan, J Cao, et al. Closed-loop control of product properties in metal forming. *CIRP Annals Manufacturing Technology*, 2016, 65(2): 573-596. https://doi.org/10.1016/j.cirp.2016.06.002.

[6] Z Zhang, R Ma, C Wang, et al. Research on springback control in stretch bending based on iterative compensation method. *Mathematical Problems in Engineering*, 2019, https://doi.org/10.1155/2019/2025717.

[7] Jianjun Wu, Zengkun Zhang. An improved procedure for manufacture of 3D tubes with springback concerned in flexible bending process. *Chinese Journal of Aeronautics*, 2020, https://doi.org/10.1016/j.cja.2020.05.036.

[8] Zengkun Zhang, Jianjun Wu, Qi Shang, et al. A new strategy for describing the characteristics of bending line in flexible push bending. *Engineering Computations*, 2019, 36(5), https://doi.org/10.1108/EC-10-2018-0475.

[9] T Ha, J Ma, J Blindheim, et al. In-line springback measurement for tube bending using a laser system. *Procedia Manufacturing*, 2020, 47: 766-773. https://doi.org/10.1016/j.promfg.2020.04.233.

[10] Yusen Li, Andi Li, Zhenming Yue, et al. Spring back prediction of AL6061 pipe in free bending process based on finite element and analytic methods. *The International Journal of Advanced Manufacturing Technology*, 2020, 109(7-8), https://doi.org/10.1007/s00170-020-05772-2.

[11] K Stelson, D Gossard. An adaptive pressbrake control using an elastic-plastic material model. *Journal of Engineering for Industry*, 1982, 104(4): 389-393.

[12] K Stelson. Real time identification of workpiece material characteristics from measurements during brakeforming. *Journal of Engineering for Industry*, 1983, 105: 45-53.

[13] K Stelson. An adaptive pressbrake control for strain hardening materials. *Journal of Engineering for Industry*, 1986, 108: 127-132.

[14] L Antonelli, P Salvini, F Vivio, et al. Identification of elasto-plastic characteristics by means of air-bending test. *Journal of Materials Processing Technology*, 2007, 183(1): 127-139.

[15] V Ton, J Havinga, V Tijum. Model-based control of strip bending in mass production. *CIRP Annals Manufacturing Technology*, 2015, 64(1): 297-300.

[16] F Dallinger, J Havinga, E Roux, et al. Adaptive process control strategy for a two-step bending process. *International Conference on Sustainable Design and Manufacturing*, 2014: 618-627.

[17] J Wang, S Verma, R Alexander, et al. Springback control of sheet metal air bending process. *Journal of Manufacturing Processes*, 2008, 10(1): 21-27.

[18] B Wei, Y Wei, F Zhang, et al. Springback control and plastic deformation of metal plates with large curvature in heat-assisted incremental bending process. *The International Journal of Advanced Manufacturing Technology*, 2021(5): 1-18. https://doi.org/10.1007/S00170-020-06492-3.

[19] Chuandong Chen, Jicai Liang, Yi Li, et al. Springback analysis of flexible stretch bending of multi-point roller dies process for Y-profile under different process parameters. *Metals*, 2021, 11(4), https://doi.org/10.3390/MET11040646.

[20] Xunzhong Guo, Yannan Ma, Wenliang Chen, et al. Simulation and experimental research of the free bending process of a spatial tube. *Journal of Materials Processing Tech.*, 2018, 255, https://doi.org/10.1016/j.jmatprotec.2017.11.062.

[21] P Groche, F Hoppe, D Hesse, et al. Blanking-bending process chain with disturbance feed-forward and closed-loop control. *Journal of Manufacturing Processes*, 2016, 24(1): 62-70. https://doi.org/10.1016/j.jmapro.2016.07.005.

[22] Zafer Tekiner. An experimental study on the examination of springback of sheet metals with several thicknesses and properties in bending dies. *Journal of Materials Processing Technology*, 2004.

[23] S Hazra, D Williams, R Roy, et al. Effect of material and process variability on the formability of aluminium alloys. *Journal of Materials Processing Technology*, 2011, 211(9): 1516-1526.

[24] J Havinga, V Ton, F Dallinger, et al. Feedforward control of sheet bending based on force measurements. *Journal of Manufacturing Processes*, 2018, 31(JAN.): 260-272. https://doi.org/10.1016/j.jmapro.2017.10.011.

[25] M Yang, N Kojima, Manabe Ki, et al. High accuracy V-bending process control with an on-line database and modified fuzzy models. *JSME International Journal*, 1997, 40(1): 157-162.

[26] M Longo, G Maccarini. Control system algorithm for the prediction of sprinback in air bending. *Key Engineering Materials*, 2013, 554-557(2): 1382-1387.

[27] D R Lewin, C Scali. Feedforward control in the presence of uncertainty. *Industrial & Engineering Chemistry Research*, 1988, 27(12): 2323-2331.

[28] M Yang, S Shima. Development of an intelligent V-bending process with a feedforward control system. *Advanced Technology of Plasticity*, 1990, 3: 1483-1488.

[29] P Groche, S Calmano, T Felber, et al. Statistical analysis of a model based product property control for sheet bending. *Production Engineering*, 2015, (1): 25-34, https://doi.org/10.1007/s11740-014-0576-5.

[30] Yongchuan Duan, Yingping Guan, Jun Zhao. Prediction and experiment verification of springback of tailor welded blanks air bending process. *Journal of Mechanical Engineering*, 2012, 48(20): 63-69. (in Chinese)

[31] Yongchuan Duan, Yingping Guan. Development of precise springback control system of tailor welded blanks air bending process. *Journal of mechanical Engineering*, 2014, 50(10): 40-47. (in Chinese)

[32] Yongchuan Duan, Le Tian, Fangfang Zhang, et. al. A fast identification method of yield strength of materials based on bending experimental data. *Metals*, 2020, 10(2): 169.